https://doi.org/10.3311/PPme.41443

Periodica Polytechnica Mechanical Engineering, 69(4), pp. 329–339, 2025

Improving Plate Performance Under Dynamic and Axial Loads Through Pre-Formed Pyramidal Structures: A Numerical Method

Akeel Zeki Mahdi[1*]

[1] College of Mechanical Engineering, University of Technology, Al-Sina'a St., Al-Wehda District/ P.O.B. 18351,10066, Baghdad, Iraq
[*] Corresponding author, e-mail: akeel.z.mahdi@uotechnology.edu.iq

Received: 28 June 2024, Accepted: 10 October 2025, Published online: 04 November 2025

Abstract

This study presents a harnessed optimization process of pre-built pyramidal modifications at enhancing the response of AISI 1010 steel planar plates subjected to simultaneous axial-dynamic loading. Unlike conventional mass adding reinforcements for enhancing buckling resistance and vibration stability. ANSYS finite element analysis featured 25 plate arrangements (pyramid heights: 0 to 20 mm; thicknesses: 1 to 3 mm), considering the boundary conditions as clamped and compression load. At increased distortion, results indicate a marked improvement in performance, particularly for thinner plates (≤2 mm). At maximum in case of deformation (h = 20 mm), critical buckling loads were improved up to 237.3%, and fundamental natural frequencies were enhanced up to 328%. The enhancements are linked to a transition from global buckling and vibration to localized modes: pyramidal regions concentrate stresses via shear band redistribution, significantly diminishing the uniformly stressed area, and limit vibrational energy by confining kinetic energy to geometric protrusions. The augmentation of performance diminishes with increasing plate thickness, exhibiting losses of 86% in buckling and 98% in frequency gains as thickness escalates from 1 mm to 3 mm. Saturation effects occur beyond h = 15 mm for thicker plates. This geometric morphing approach provides a resource-efficient transformation for lightweight structural construction.

Keywords

geometric optimization, stability of vibration, buckling resistance, pyramidal formations, lightweight of structures

1 Introduction

Thin-walled structural components are especially prone to buckle and vibration failures under dynamic and axial pressures. Hence, performance improvement has been investigated widely. The spring plate model by Wu et al. [1] was among the first analytical frameworks to explain dynamic instability, followed by several other methodologies later on. This covers the use of piezoelectric transducers for predicting buckling of structures [2], the use of signal processing for transient vibration [3] etc., to the integrated approach of being able to predict buckling loads non-destructively using the vibration correlation method [4]. Extra difficulty rises in multi-physics states, demonstrated via the thermo-acoustic volatilities inspected through Sha et al. [5] and also the thermal sensitivity of functionally arranged materials considered by Ramkumar and Ganesan [6]. These notions, combined into computational techniques, proved by Muthu Kumar et al. [7], have more improved synchronized stability vibration forecasts.

Simultaneously, pure buckling phenomena are localized and extensively studied across different materials and geometries. Numerical- experimental assessments of composite tubes [8], theoretic investigations of hardened cylindrical shells [9], and research into the buckling strength of polygonal sections [10] are all examples of the investigations being carried out. Critical stresses have been improved with advanced plate theories [11], and digital methods have defined formability limits [12]. Changes range from fundamental to material, with an elaborate inspection in high-strength steel revealing conservatism of design codes [13] as well as higher-strength material showing less than intuitive buckling patterns [14]. Validation studies that confirm the capability of finite element software in performing stability analysis often back the reliability of these numerical analyses [15–17].

Despite this extensive work, a typical feature of traditional reinforcement methods is their reliance on large structural

Cite this article as: Zeki Mahdi, A. "Improving Plate Performance Under Dynamic and Axial Loads Through Pre-Formed Pyramidal Structures: A Numerical Method", Periodica Polytechnica Mechanical Engineering, 69(4), pp. 329–339, 2025. https://doi.org/10.3311/PPme.41443

alterations such as additional stiffeners, composite layers, or material grading or on complex sensing systems. Each one often contests with the core aim of lightweight design. This leads to a clear research gap for structural performance enhancement techniques that preserve the mass as well.

In this study, a new approach based on the use of predefined geometric capital i.e., pyramidal distortions, to address this disparity. Rather than increasing mass, this thickness-preserving strategy profoundly alters structural performance over state of the art approaches. This work demonstrates that this method also enhances buckling resistance (critical load multipliers increased up to 237.3%) and vibration stability (fundamental frequencies increased up to 328%) in AISI 1010 steel plates under axial-dynamic loading. An example of a resource-efficient way to construct lightweight structures, this dual-performance paradigm change is achieved entirely passively through controlled geometric morphing.

2 Methodological framework

An AutoCAD 2022 square plate of size 50 × 50 cm with varying thicknesses of 1, 1.5, 2, 2.5, and 3 mm was designed. For initial work, flat plates were distorted at their centers in a pyramidal fashion, such that each had uniform thickness and pyramidal heights of 0, 5, 10, 15, and 20 mm. This procedure led to a matrix of 25 configurations, consisting of five undeformed plates (0 mm of height h), used to study the effects of height and thickness. The AISI 1010 steel material referenced in [18] was used with E = 205 Gpa (modulus of elasticity), σ_{yield} = 285 MPa, v = 0.29 (Poisson's ratio), and ρ = 7870 kg/m^3 (density).

Buckling and vibration were analyzed using ANSYS 2017 as part of the finite element analysis process. The various boundary conditions are implemented as given below: Left and right edges are fully enforced (all degrees of freedom fixed). The top and bottom edges are free to move only in the y direction, but they cannot be moved in the x and z directions. Buckling was induced by applying a 1500 N axial compressive load at the top and bottom edges in opposite directions. That corresponds to 60% of Timoshenko's critical buckling load for flat plates, Eq. (1) [19], so that buckling modes are activated without yielding, preventing inelastic deformation for vibration applicability limits, and that direct performance comparisons are possible throughout all tested thicknesses (1-3 mm) and also throughout all tested deformation heights (0-20 mm).

$$F_{cr} = \frac{4\pi^2 E}{12\left(1-v^2\right)}\left(\frac{t}{b}\right)^2 A_{edge}\,, \tag{1}$$

where: F_{cr} is the critical buckling load (N), t is the thickness of the plate (m), b is the length of the square plate (0.5 m), and A_{edge} is the area of the edge (A = 0.5 × t) (m^2).

The 1500 N force was translated to pressure values for each plate configuration to account for geometric changes, Eq. (2), considering thickness-dependent edge areas and pyramidal tilt angles.

$$\text{Pressure}\left(\text{Pa}\right) = \frac{1500N}{0.5\times t\times\cos\left(\begin{array}{l}\text{angle of}\\ \text{tilt of plate}\end{array}\right)} \tag{2}$$

As illustrated in (Table 1). The boundary conditions and load applied as pressure are exhibited in (Fig. 1).

Modal analysis determined the initial six natural frequencies and corresponding mode shapes. A consistent (15 mm) triangular mesh was utilized throughout all models (Fig. 2), comprising 28,253 nodes and 13,801 elements for t = 1 mm, h = 0 mm, while 28,784 nodes for t = 1 mm, h = 6 mm. Mesh convergence was confirmed (Fig. 3).

2.1 Strategy of buckling eigenvalue analysis

The numerical approach was validated by means of benchmark studies on buckling of thin plates [17]. Critical buckling stresses of the first six modes were determined by a linear eigenvalue analysis in ANSYS. The method solves the characteristic equation $[K] - \lambda[S]\{\psi\} = 0$, where $[K]$ is the stiffness matrix, $[S]$ is the stress stiffness matrix, λ is the load multiplier, and $\{\psi\}$ is the eigenvector (mode shape). Though all six modes were examined, the primary focus

Table 1 Pressure values corresponding to the force of 1500N for each edge area of the plate

Plate thickness t (mm)	Pressure (kPa) at h = 0 mm	Pressure (kPa) at h = 5 mm	Pressure (kPa) at h = 10 mm	Pressure (kPa) at h = 15 mm	Pressure (kPa) at h = 20 mm
1.0 mm	3000	3001.8	3007.2	3016.2	3028.8
1.5 mm	2000	2001.2	2004.8	2010.8	2019.2
2.0 mm	1500	1500.9	1503.6	1508.1	1514.4
2.5 mm	1200	1200.72	1202.88	1206.48	1211.52
3.0 mm	1000	1000.6	1002.4	1005.4	1009.6

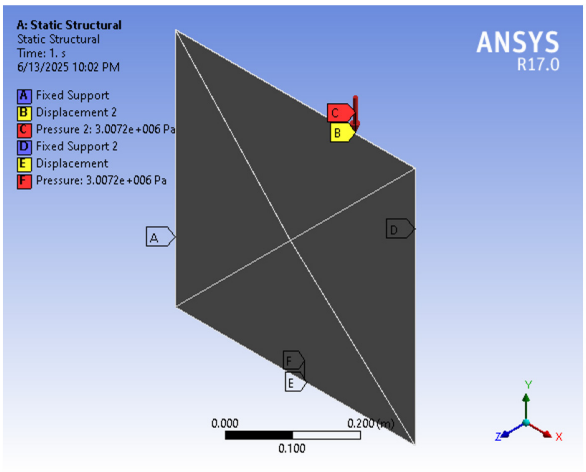

Fig. 1 The boundary conditions and load applied as pressure (For representative plate: t = 1 mm, h = 10 mm)

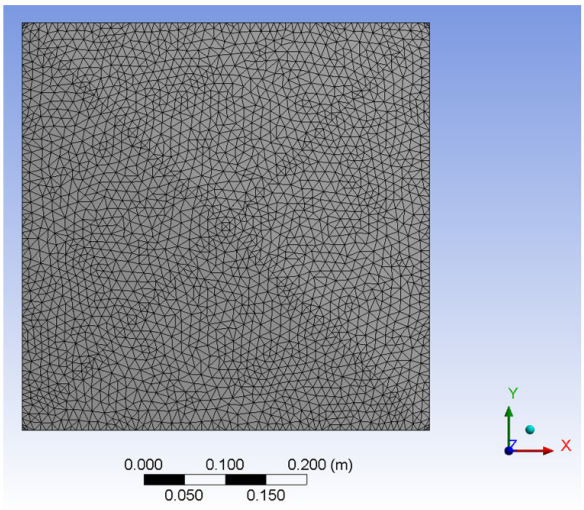

Fig. 2 Plate mesh configuration (For representative plate: t = 1 mm, h = 10 mm)

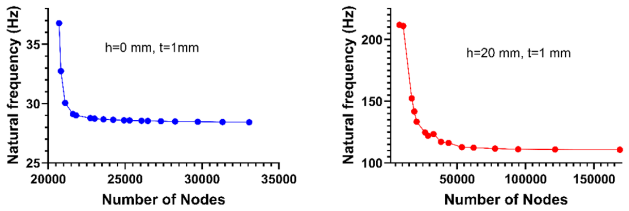

Fig. 3 Mesh convergence study- Natural frequency vs. number of nodes (For representative plate: t = 1 mm, h = 0 mm, and h = 20 mm)

was placed on Mode 1 (the basic buckling mode), as it corresponds to the most severe mode of failure under compression. In order to evaluate the enhancement of buckling resistance, we performed a semi-systematic investigation in which we studied the effect of plate thickness (1-3 mm) and deformation height (0-20 mm) on λ_{cr}.

2.2 Strategy of model (vibration) analysis

An eigenvalue analysis, also known as modal analysis, was performed to acquire natural frequencies without the consideration of stress stiffening effects from the compressive load of 1500 N. Where the governing equation $[K] - \omega^2[M]\{\phi\} = 0$ was solved, $[K]$ is the stiffness matrix of the pre-stressed, $[M]$ is the mass matrix. ω is the angular frequency, and $\{\phi\}$ is the vibration mode shape. The six modes were detected, but the research primarily investigated natural frequency (f_1) due to the major impacts on dynamic response. The modifications in thickness (t) and deformation height (h) were associated with the changes that occurred in (f_1) to assess the improvements in vibration stability and to properly reflect the actual working environment.

3 Results and discussions

3.1 Buckling performance

It is shown through parametric buckling analysis that the pyramidal deformations are essential to modifying the failure modes and that the critical buckling performance is dramatically improved. This is in accordance with the geometric reinforcing rules that have previously been discovered in CFRP structures [8] and functionally graded materials [6]. Table 2 quantifies the exponential growth of the load multiplier (λ_1) with respect to deformation height (h), and finds that for thin plates ($t \leq 2$ mm). The peak increase of 237.3% (t = 1 mm, h = 20 mm) demonstrates that at sufficient length scale, the approach of geometric reinforcement transcends that of material-addition methods (Eq. (3)). The enhancements were consistent with thickness-dependent efficiency trends observed in shear-inclusive plate theories [11] and corroborated through digital twin analyses [12]. Data aggregation shows that thin plates enjoy higher benefit, i.e., 237% at t = 1 mm against 151% at t = 3 mm when h = 20 mm.

$$\text{Improvement}\% = \left(\frac{\left|\lambda_{(h,t)}\right| - \left|\lambda_{(h=0,t)}\right|}{\left|\lambda_{(h=0,t)}\right|} \right) \times 100 \tag{3}$$

Fig. 4 shows the process of geometric reinforcement. For plates equal to or less than 2 mm, pyramidal distortions greatly enhance the effective second moment of area and allow a corrugated profile to effectively restrain buckling through membrane action. The key element of this geometric advantage is extremely responsive in situations when the foundation plate has low bending stiffness in the inherent sense. In the stiffer matrices of thicker plates, however, this built-in stiffness dominates the system response, rendering distortions less impactful and resulting in the observed

Table 2 The critical load multiplier (λ_1) and improvement (%)

t (mm)	Parameter	h = 0 mm	h = 5 mm	h = 10 mm	h = 15 mm	h = 20 mm
1	λ_1	2.064	12.629	16.274	16.851	17.304
	Improvement	---	161%	216%	227%	237%
1.5	λ_1	6.963	37.013	40.217	44.476	45.262
	Improvement	---	109%	163%	181%	189%
2	λ_1	16.5	29.697	87.974	99.579	98.87
	Improvement	---	80%	139%	162%	171%
2.5	λ_1	32.21	51.997	168.24	172.9	190.74
	Improvement	---	61%	120%	148%	161%
3	λ_1	55.64	82.682	287.82	289.97	300.33
	Improvement	---	49%	104%	135%	151%

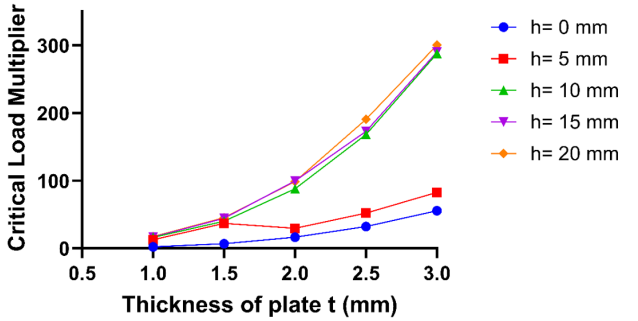

Fig. 4 Critical load multiplies vs thickness of plate for variable height h

plate performance saturation. The dependence on the thickness is in agreement with observations in [13] and [6]. The critical change at t = 2 mm shows λ_1 increases by 432% over (h = 0 to 10 mm) or only 197% at t = 3 mm - demonstrating the drastically higher level of geometric flexibility within thin plates. We find improvement percentages concerning plate thickness (Fig. 5), and the indicated optimal volatility and good fitting are increasing gain (≥200%) at $t \leq 1.5$ mm ($h \geq 15$ mm), which explicitly depicts the optimization threshold. The substantial 86% decrease in improvement from 237% to 151% (h = 20 mm) as thickness increases from 1 to 3 mm demonstrates the diminishing

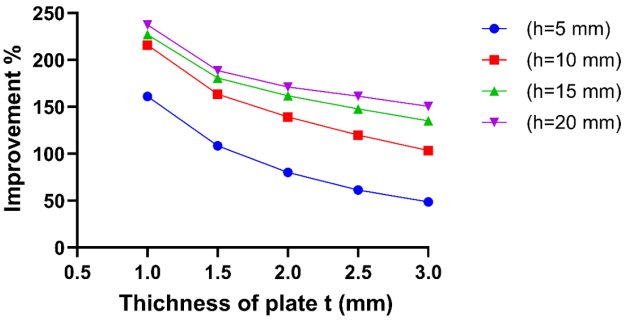

Fig. 5 Improvement in load multiplies vs thickness of plate for variable height h

returns of plates with ever-thicker plates, thus favoring thin-plate applications and confirming the observations made regarding tension-driven buckling processes [14].

Analysis of λ_1 versus height of deformation, at the same time, 98.87 versus 87.97 at h = 20 mm and h = 10 mm for t = 2 mm, respectively (more than 90% of total benefits was obtained over the distance between those two lines exposed in (Fig. 6), shows the elevated stiffening behind h = 10 mm. The saturation effect observed with increasing thickness (t≥2.5 mm) when h = 15 mm, where λ_1 plateaued at 5% corresponds to the reduced geometric compliance. An increase in the distortion height brings the material in the sharp corners of the pyramids close to its yield stress limit (285 MPa for AISI 1010), and localized plastic yielding is initiated. This situation prevents further redistribution of elastic energy and consequently a further increase in stiffness. The strength limit of the material approaches or surpasses what can be gained geometrically; therefore, the potential to increase buckling resistance by adding more material is limited. For thicker plates (t > 2.5 mm), saturation effects in h > 15 mm relate to reduced geometric compliance, with plastic yielding at pyramid vertices (AISI 1010, yield stress = 285 MPa) limiting further elastic energy redistribution. Improvement percentages

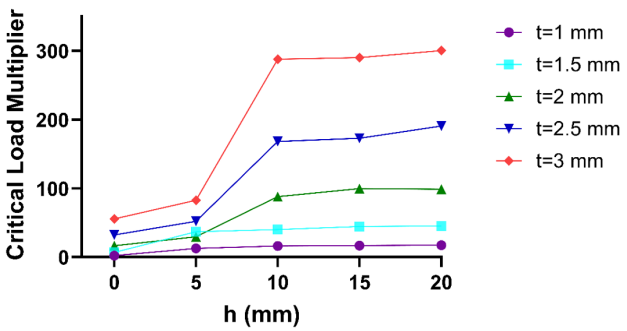

Fig. 6 Critical load multiplies vs height h for variable thickness of plate

are averaged over 10 different ratios of r and trend with h (Fig. 7) and show a diminishing marginal utility for thicker plates: at t = 3 mm, the returns plateau from 135% (h = 15 mm) to 151% (h = 20 mm); only a mere 12% more return for a 33% increase in height. In contrast, the ongoing amplification rate of 22% per 5 mm for t = 1 mm is essentially constant, which would result in simple linear-phase behavior, thus allowing reinforcements to be predicted and designed in a predictable manner, akin to a spring-plate concept [1].

There are three different regimes over which buckling modes progress (Fig. 8). At zero deformation (h = 0), it is classical global buckling seen as full plate bending with a uniform stress state (see Fig. 8(a)), consistent with classical Timoshenko's theory [19]. At h = 5 mm (Fig. 8(b)), stress concentration localized at the base of the pyramidal yields to the generation of diagonal shear bands. Such bands transmitted applied stresses through localized plastic deformation mechanisms, thus increasing the size of the unstressed zone [18] and reducing the effective cross-sectional area within the band that can carry loads. When $h \geq 10$ mm (Figs. 8(c)-(e)). Parallelized efficient load path optimization in rigid shells [9] Diamond wrinkling confines deformation to pyramidal areas, and localized stability and load-path optimization reallocate load from pyramid peaks to edges, improving critical buckling resistance 5.3 (t = 2 mm, h = 10 mm vs. h = 0 mm).

3.2 Characteristics of vibrational behavior

Pyramidal plates are among the effective devices to upscale natural frequencies of the system due to their significant amplification in the first mode (f_1), which dominates structural reaction because of its lowest energy state and largest susceptibility to any excitation. This data is aligned with the vibration-buckling correlations found in semi-empirical approaches [4] and [6]. Using Eq. (4),

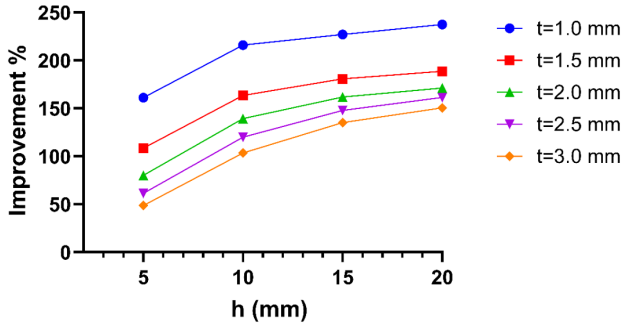

Fig. 7 Improvement in load multiplies vs height h for variable thickness of plate

the percent increase in natural frequency compared to flat plates (h = 0) is given as follows:

$$\text{Improvement\%} = \left(\frac{f_{(h,t)} - f_{(h=0,t)}}{f_{(h=0,t)}} \right) \times 100 \tag{4}$$

The first-mode natural frequency (f_1) of the buckled structure has been significantly enhanced according to the exponential increase as shown in Table 3, and a 328% maximum enhancement has been reached (121.98 Hz compared to 28.49 Hz at h = 5 mm, for thiner plate (t = 1 mm, h = 20 mm). The thickness-dependent increases are consistent with trends expected in [6] and [7]. The combined data shows that the negative thickness dependence is still present: thinner plates exhibit considerably higher gains (328% at t = 1 mm, versus 230% at t = 3 mm, h = 20 mm). This confirms that the impact of geometric reinforcement diminishes with additional plate thickness.

The relationship between natural frequency (f_1) and plate thickness also has a nonlinear growth, as shown in (Fig. 9). This means that a decrease of the expansion height (h) from 20 mm to 10 mm or even lower will cause an increase in f_1 = 28.5 Hz (t = 1 mm) to 282.1 Hz (t = 3 mm) at the maximal deformation height (h = 20 mm). Greatest sensitivity is reached for the t = 1.5-2 mm replication region, indicating this thickness domain offers optimal frequency tuning ability. It applies to applications for flat plates [2]. This phenomenon can also be represented through percentage improvement, as depicted in (Fig. 10), where all of the percentage enhancements for thin plates ($t \leq 1.5$ mm and $h \geq 15$ mm) exceed the threshold of 313%. Finally, it is worth mentioning the 98% drop in gains (328% to 230%) as thickness increases from 1 to 3 mm (h = 20 mm), which clearly illustrates the diminishing returns of increasing the size of setups. At high frequencies, below h = 10 mm, we see a rapid increase attributed to localized stiffness due to curvature at pyramid vertices, with these effects greatly increasing natural frequencies, with geometric rigidity greatly increasing natural frequencies, as illustrated in (Fig. 11). A higher degree of stiffness in relation to the serial half-tube leg pair is quickly formed without additional mass being added. This is due to localized stress concentrations reaching material strength limits beyond h = 15 mm, stepping leads to decreased return in stiffness, illustrating one optimization limit: for this method of reinforcing. For $t \geq 2$ mm, this saturation drags the further increases to ≤5% beyond h = 15 mm. Which corresponds with the research findings [5]. This trend is manifested in the following improvement percentages (Fig. 12),

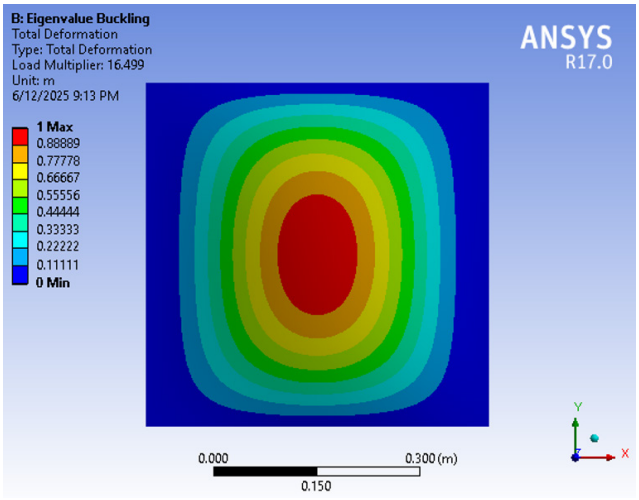

(a)

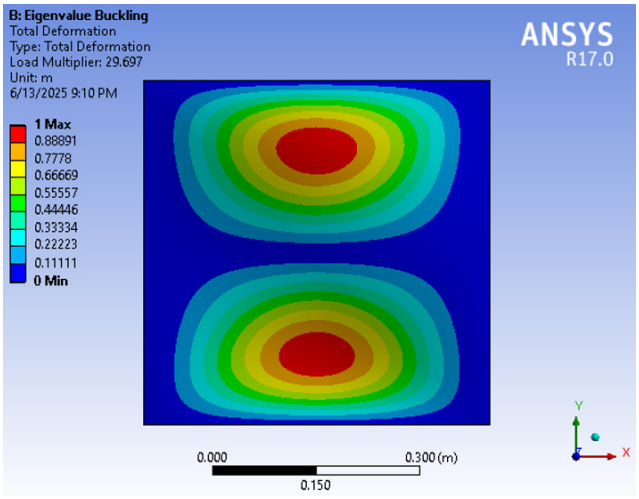

(b)

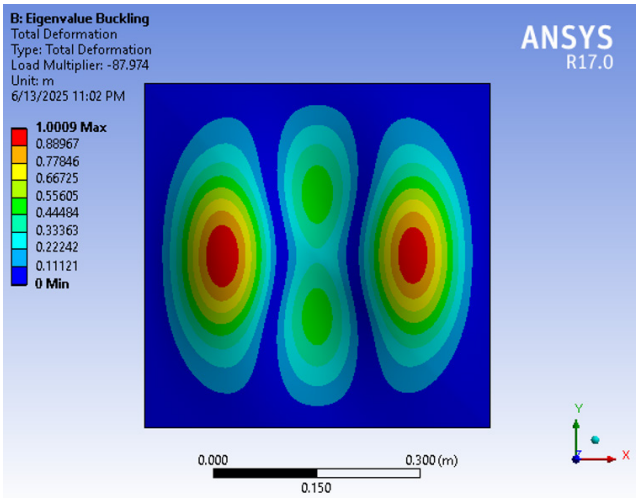

(c)

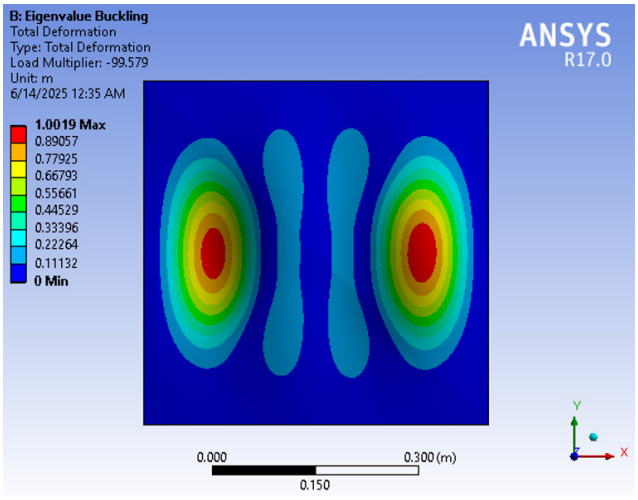

(d)

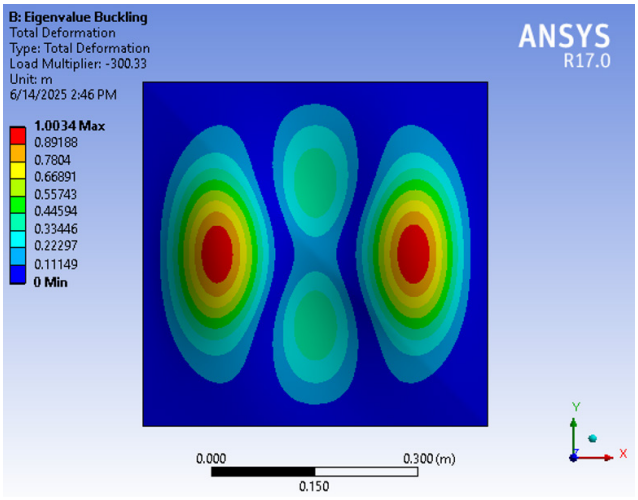

(e)

Fig. 8 Critical load multiplies buckling mode of shape (For representative plate: $t = 2$ mm, $h = 0$-20 mm): (a) $h = 0$, $t = 2$ mm, (b) $h = 5$, $t = 2$ mm, (c) $h = 10$, $t = 2$ mm, (d) $h = 15$, $t = 2$ mm, (e) $h = 15$, $t = 2$ mm

Table 3 The Natural frequency f_1 (Hz) and improvement (%)

t (mm)	Parameter	h = 0 mm	h = 5 mm	h = 10 mm	h = 15 mm	h = 20 mm
1	f_1 (Hz)	28.494	84.611	113.49	117.64	121.98
	Improvement	---	197%	298%	313%	328%
1.5	f_1 (Hz)	42.739	96.846	142.91	159.69	163.04
	Improvement	---	127%	234%	274%	281%
2	f_1 (Hz)	56.982	107.33	165.98	197.48	210.04
	Improvement	---	88%	191%	247%	269%
2.5	f_1 (Hz)	71.222	117.47	182.51	225.41	251.28
	Improvement	---	65%	156%	217%	253%
3	f_1 (Hz)	85.459	127.75	192.61	248.03	282.12
	Improvement	---	50%	125%	190%	230%

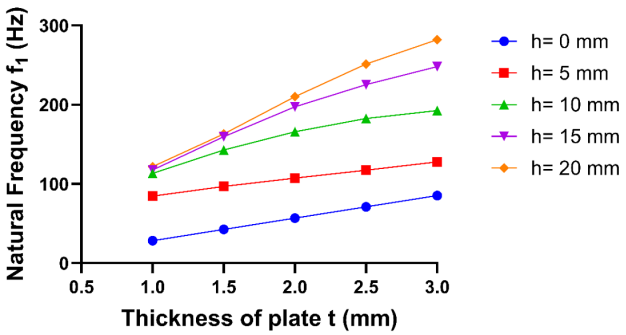

Fig. 9 Natural frequency f_1 vs thickness of plate for variable height h

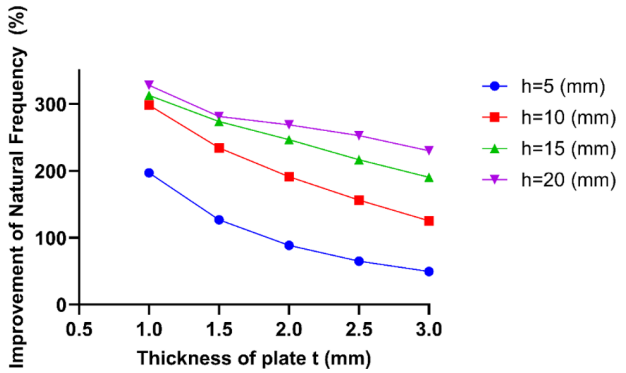

Fig. 10 Improvement of Natural frequency f_1 vs thickness of plate for variable height h

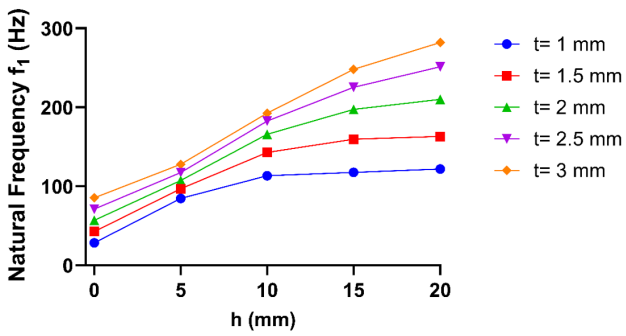

Fig. 11 Natural frequency f_1 vs height h for variable thickness of plate

with only near-linear gains for thin plates (t = 1 mm), but determined gains for thicker plates (t = 3 mm), yielding a total gain of only 40% compard to the full h = 5 to 20 mm range. Energy progression of the vibrational modes towards deformation height. This implies a radical reshaping of global harmonics (Fig. 13). From the fully decoupled (Fig. 13(a): h = 0) to strongly coupled full-plate oscillation at near-uniform displacement, a variety of dynamic coupling occurs (Fig. 13(b): h = 5 mm), indicates partial confinement to the base of the pyramid with ±45° antinodes and localized vibration (Fig. 13(c)-(e): $h \geq 10$ mm) [7] thereby refining mass-restriction concepts. collimates energy at pyramid vertices, reduces effective mass participation by approximately 40%, and increases f_1 by 3.3 vs. flat plates (t = 1.5 mm, h = 15 mm vs. h = 0). could be put at the end higher-order vibrational modes (2-6) exhibit complex nodal structures, as shown in (Fig. 14). Though these modes show complex wavefronts with diamond-shaped contours in, for example, Mode 2, their role in the fundamental response is secondary (f_1 = almost 70% of total kinetic energy), and this ranking was similar to those reported in [2] for dynamic cases. It is this physical advantage that makes first-mode behavior the preferred state in applications that sensibly detect vibration.

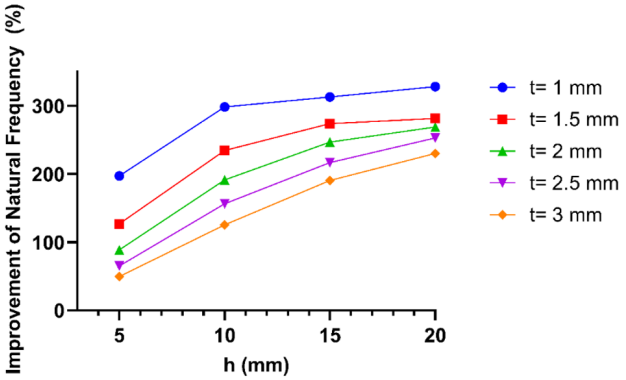

Fig. 12 Improvement of Natural frequency f_1 vs height h for variable thickness of plate

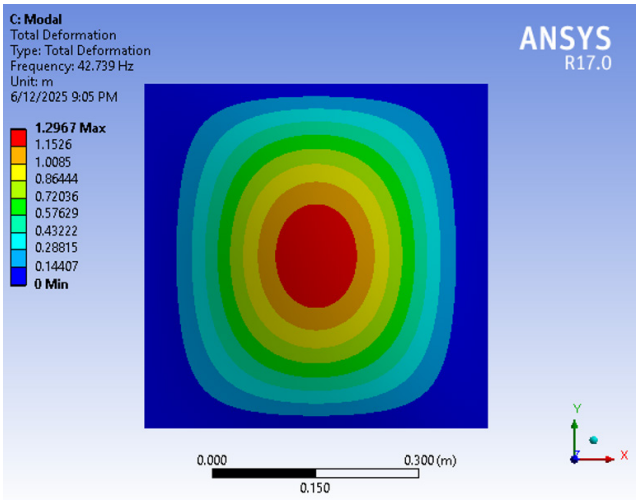

(a)

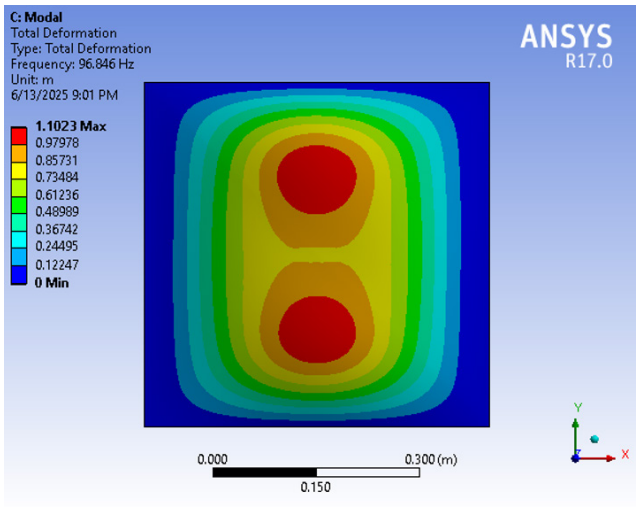

(b)

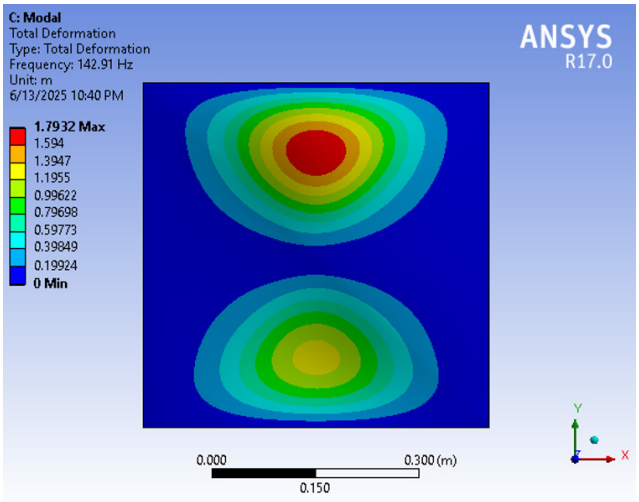

(c)

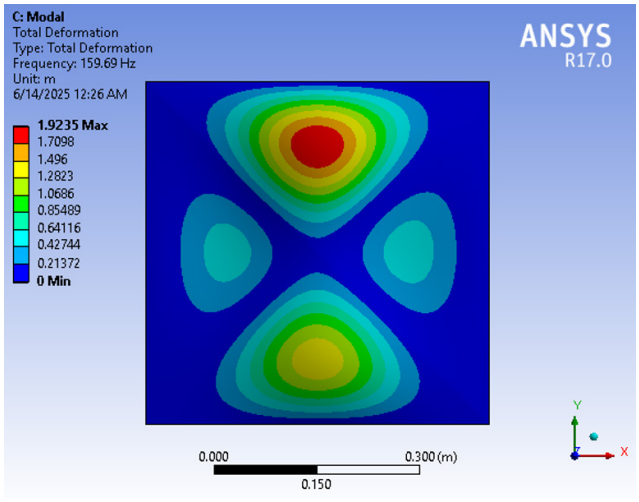

(d)

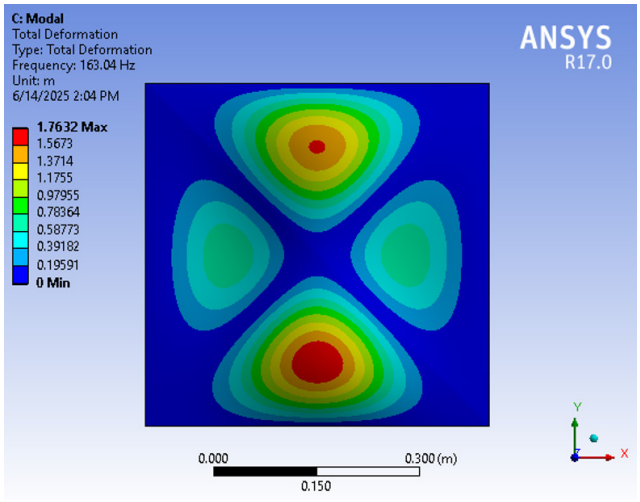

(e)

Fig. 13 Natural frequency f_1 and mode of shape (For representative plate: t = 1.5 mm, h = 0-20 mm): (a) $h = 0$, $t = 1.5$ mm, (b) $h = 5$, $t = 1.5$ mm, (c) $h = 10$, $t = 1.5$ mm, (d) $h = 15$, $t = 1.5$ mm, (e) $h = 15$, $t = 1.5$ mm

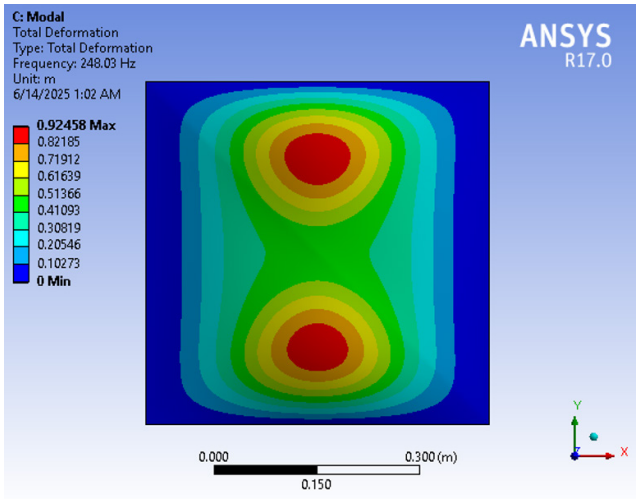

(a)

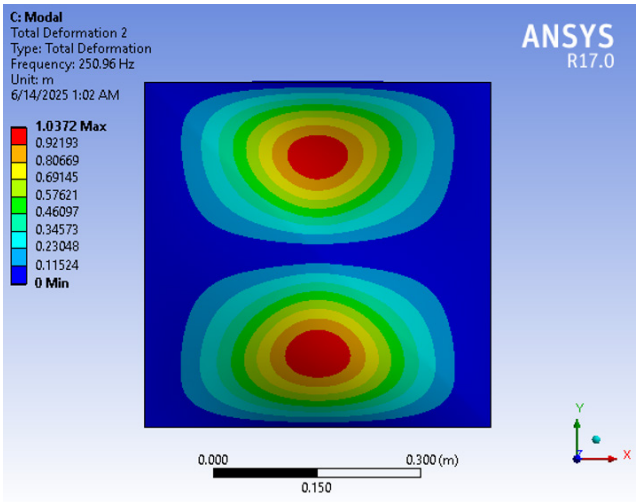

(b)

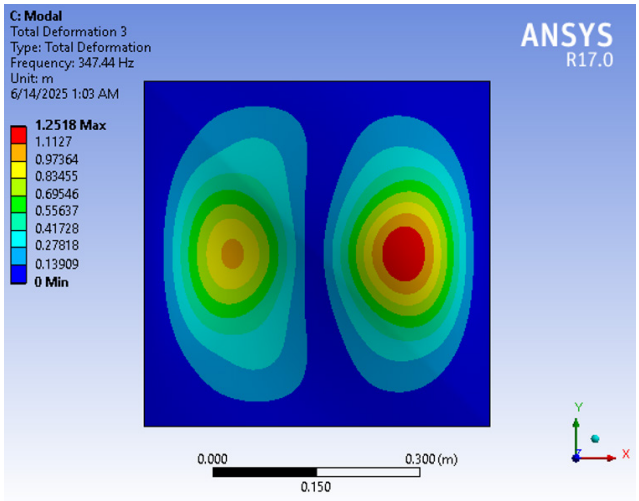

(c)

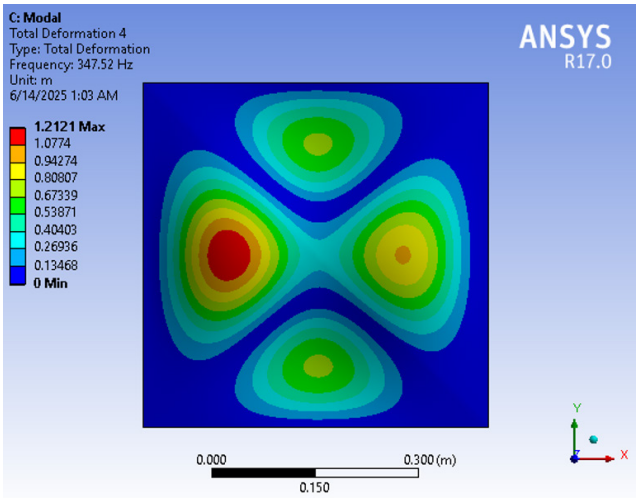

(d)

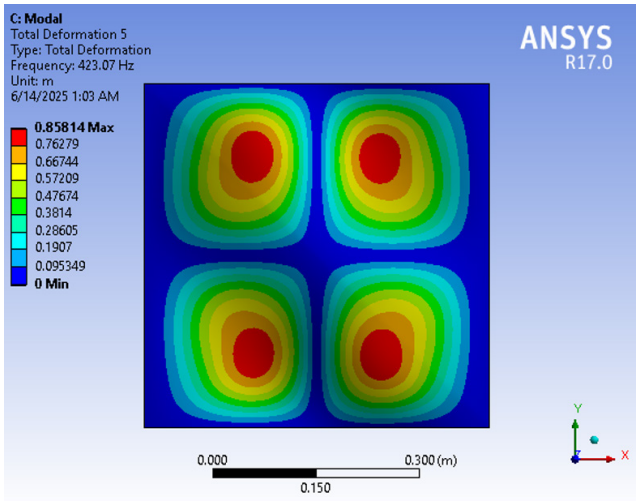

(e)

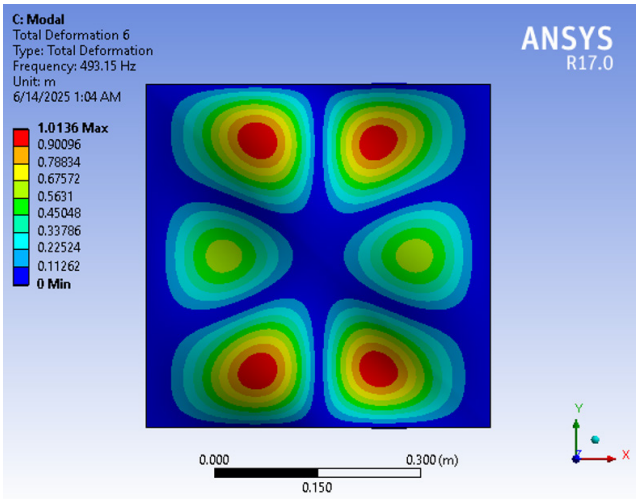

(f)

Fig. 14 mode of shape (For representative plate: $t = 3$ mm, $h = 10$ mm): (a) 1st mode of shape of vibration, (b) 2nd mode of shape of vibration, (c) 3rd mode of shape of vibration, (d) 4th mode of shape of vibration, (e) 5th mode of shape of vibration, (f) 6th mode of shape of vibration

4 Conclusions

This investigation fully demonstrates the dual-enhancement technique of pre-formed pyramidal imperfections in reinforcing the buckling resistance as well as the dynamic stability of thin plates made of steel. The primary conclusions affirm that:

1. Pyramidal distortions improve buckling resistance by as much as 237.3% and fundamental natural frequency by up to 328% without increasing mass, exceeding conventional reinforcement techniques that generally necessitate material augmentation.
2. The efficiency shows significant thickness dependence, with thin plates (≤1.5 mm) displaying the greatest enhancements (>200%), whilst bigger plates (≥2.5 mm) reveal diminishing returns due to less geometric flexibility.
3. At a threshold height of 10 mm, local diamond buckling wrinkle formation and vertex energy localization, in vibration, fundamentally alter structural performance by promoting load paths and reducing effective mass participation; however, the thicker the plates, the more performance saturation of the above-described lower and higher vibration mode occurs (≥15 mm).
4. This method provides consistent and predictable improvement of thin sheets, leading to a linear frequency increase of 22% per 5 mm height increase at t = 1 mm, thus enabling formulation of clear design limits (h = 15 mm, $t \leq 1.5$ mm) for lightweight applications.

This numerical investigation shows the fundamental effectiveness of the approach, but it's important to acknowledge its significant limitations. The present boundary conditions and loading configuration represent idealized conditions that will not completely represent complicated real-world applications. Future studies should focus on experimental testing using three-dimensional digital image correlation and manufacturability evaluation based on stamping experiments. Additionally, performance under less-than-ideal boundary conditions, including partial fixity and complex loading conditions, will confirm the applicability of this geometric reinforcement method for lightweight structural systems. Such initiatives would link numerical validation with physical implementation, at least within the frame of the case of interest, especially for cases when weight is of paramount importance, be it in aeronautics, space, or medical applications.

References

[1] Wu, M., Zhu, J., Huang, X. "An analytical solution for dynamic instability and vibration analysis of structural members with open and closed sections", Scientific Reports, 15(1), 5152, 2025. https://doi.org/10.1038/s41598-025-85708-6

[2] Moharana, S., Bhalla, S., Munjwani, S. "Vibration-based pre-emptive detection of plate buckling using piezo-transducers", Innovative Infrastructure Solutions, 7(3), 188, 2022. https://doi.org/10.1007/s41062-022-00749-4

[3] Li, Z., Xu, W., Wang, C., Liu, X., Sun, Y. "Investigation on Vibration Characteristics of Thin-Walled Steel Structures under Shock Waves", Materials, 16(13), 4748, 2023. https://doi.org/10.3390/ma16134748

[4] Sukajit, P., Singhatanadgid, P. "Identification of buckling load of thin plate using the vibration correlation technique", In: 21st Conference of Mechanical Engineering Network of Thailand, Chonburi, Thailand, 2007, pp. 17–19.

[5] Sha, Y. D., Gao, Z. J., Xu, F., Li, J. Y. "Influence of thermal loading on the dynamic response of thin-walled structure under thermo-acoustic loading", Advanced Engineering Forum, 2–3, pp. 876–881, 2011. https://doi.org/10.4028/www.scientific.net/AEF.2-3.876

[6] Ramkumar, K., Ganesan, N. "Finite-element buckling and vibration analysis of functionally graded box columns in thermal environments", Proceedings of the Institution of Mechanical Engineers, Part L: Journal of Materials: Design and Applications, 222(1), pp. 53–64, 2008. https://doi.org/10.1243/14644207JMDA129

[7] Kumar, R. C. M., Jacques, B. P. S., Ádány, S., Avci, O., Hajjar, J. F., Schafer, B. W. "Efficient stability and vibration analysis of an all-steel modular floor assembly", In: Proceedings of the SSRC Annual Stability Conference, Chicago, USA, 2023, pp. 1–20.

[8] Różyło, P., Rosłaniec, K., Kuciej, M. "Buckling of compressed thin-walled composite structures with closed sections", Advances in Science and Technology Research Journal, 17(6), pp. 63–72, 2023. https://doi.org/10.12913/22998624/174193

[9] Hoshide, K., Chun, P. J., Ohga, M., Shigematsu, T. "Buckling strength of thin-walled steel cylindrical shells with stiffened plates", IOP Conference Series: Materials Science and Engineering, 504(1), 012091, IOP Publishing. 2019. https://doi.org10.1088/1757-899X/504/1/012091

[10] Kobashi, T., Ikarashi, K., Kanno, R., Nakayasu, N., Shimizu, N. "Local Buckling Strength of Octagon Tubular Steel Member", In: 7th International Conference on Coupled Instabilities in Metal Structures, Baltimore, MD, USA, 2016.

[11] Piscopo, V. "Refined buckling analysis of rectangular plates under uniaxial and biaxial compression", International Journal of Mechanical, Industrial and Aerospace Sciences, 4(10), pp. 554–561, 2010.

[12] Almeida, I. M., Magrinho, J. P., Silva, M. B., Martins, P. A. "Formability limits by local buckling in thin-walled tubes and profiles", Materials Research Proceedings, 54, pp. 1061–1068, 2025. https://doi.org/10.21741/9781644903599-115

[13] Lei, G., Ming, N., Xingkun, X., Linyue, B., Lixiang, H. "Local and Global Interactive Buckling Capacity of Thin-Walled Box-Section Members of BS700 High-Strength Steel under Axial Compression", Advances in Materials Science and Engineering, 2022(1), 9259324, 2022. https://doi.org/10.1155/2022/9259324

[14] Kilardj, M., Ikhenazen, G., Messager, T., Kanit, T. "Linear and nonlinear buckling analysis of a locally stretched plate", Journal of Mechanical Science and Technology, 30(8), pp. 3607–3613, 2016.

[15] Hassan, A. H. A., Kurgan, N. "Modeling and buckling analysis of rectangular plates in ANSYS", International Journal of Engineering and Applied Sciences, 11(1), pp. 310–329, 2019. https://doi.org/10.24107/ijeas.531011

[16] Chen, B. O., Sivakumaran, K. S. "Post-buckling shear strength of thin steel plates", Procedia Engineering, 14, pp. 641–647, 2011. https://doi.org/10.1016/j.proeng.2011.07.081

[17] Pouladkhan, A. R., Emadi, J., Safamehr, M. "Numerical study of buckling of thin plates", World Academy of Science, Engineering and Technology, 78(1), pp. 152–157, 2011.

[18] ASM Handbook Committee "Hardenability Curves", In: Properties and Selection: Irons, Steels, and High-Performance Alloys, ASM International, 1990. ISBN 978-1-62708-161-0 https://doi.org/10.31399/asm.hb.v01.a0001030

[19] Timoshenko, S. P., Gere, J. M. "Theory of Elastic Stability", McGraw-Hill, 1961.